Journal of Solid State Chemistry 183 (2010) 1297–1302

Contents lists available at ScienceDirect

Journal of Solid State Chemistry

journal homepage: www.elsevier.com/locate/jssc

Structure determination of α-$La_6W_2O_{15}$

M-H. Chambrier [a], R.M. Ibberson [b,1], F. Goutenoire [a,*]

[a] Laboratoire des Oxydes et Fluorures, UMR-CNRS 6010, Université du Maine, 72085 Le Mans Cedex 9, France
[b] ISIS Facility, STFC–Rutherford Appleton Laboratory, Harwell Science and Innovation Campus, Didcot OX11 0QX, UK

ARTICLE INFO

Article history:
Received 14 December 2009
Received in revised form
17 March 2010
Accepted 25 March 2010
Available online 8 April 2010

Keywords:
Oxide
X-ray and neutron diffraction
Phase transition

ABSTRACT

The structure of the high temperature alpha form of $La_6W_2O_{15}$ has been determined ab-initio from high temperature laboratory X-ray and neutron time-of-flight data. This tungstate crystallizes in the non-centrosymmetric orthorhombic space group (No. 20) $C222_1$, with $Z=2$, $a=12.6250(2)$ Å, $b=9.1875(1)$ Å, $c=5.9688(1)$ Å. The structure comprises $[O_2La_3]$ infinite ribbons and is better described by the structural formula $[O_2La_3]_2[WO_{5.5}]_2$. Using this description we can understand the strong structural similarity of the present compound with compounds of the general composition BiM_2AO_6 (M=Cu, Mg, Zn, Mn, Cd, Ca, Pb; A=P, As, V) described as $[O_2M_2Bi][AO_4]$. The $[WO_{5.5}]$ entity implies oxygen disorder in the material.

1. Introduction

The La_2O_3–WO_3 phase diagram has been studied by a number of groups; for example, Yoshimura [1], Yanoskii [2] and Ivanova [3]. In these studies, little detailed crystallographic information was reported due to the lack of good single crystals. Following recent crystallographic investigations on the La_2O_3–MoO_3 system, using high-resolution powder diffraction to determine the structures of $La_2Mo_4O_{15}$ [4], $La_6Mo_8O_{33}$[5] and $La_2Mo_2O_9$[6], we now focus our work on the La_2O_3–WO_3 phase diagram in an effort to characterise potentially important crystal structures in this system. During the re-investigation of the La_2O_3–MoO_3 system, oxygen ion conduction was discovered in $La_2Mo_2O_9$ [7] and in the high temperature form of $La_2W_2O_9$ [8]. The structure of $Bi_6Cr_2O_{15}$ with a similar formula also presents limited ionic conduction by oxygen atoms [9]. These observations lead us to explore the structure of title compound. $La_6W_2O_{15}$ has phase transitions at 630 and 930 °C as previously reported [1–3]. The only crystallographic information available is two sets of unit cell parameters: a B-centered orthorhombic cell $a=25.25$ Å, $b=11.917$ Å, $c=17.824$ Å by Yoshimura (PDF-File 031-0674) and a primitive orthorhombic cell $a=8.93$ Å, $b=12.65$ Å, $c=5.97$ Å by Yanovskii (PDF-File 037-0124).

Here we present the structure determination of the high-temperature form, α-$La_6W_2O_{15}$, and the thermal evolution of the cell parameters of the sub-lattice for the lower temperature beta and gamma forms. We will find that the present compound is related to $BiMg_2PO_6$ but with additional oxygen atoms.

2. Experimental

Room temperature and the high-temperature X-ray diffraction patterns were collected on a Bragg-Brentano diffractometer (MPD-PRO Panalytical) equipped with a linear detector X'Celerator and an Anton Paar HTK12 furnace. The high-temperature X-ray diffraction patterns were collected overnight, 2 theta range [12–60°] from 40 to 1040 °C and to 1040 to 200 °C/Step 40 °C, 20 min/pattern. Time-of-flight neutron diffraction data were collected on the high resolution powder diffractometer, HRPD, at the ISIS pulsed neutron source, Rutherford Appleton Laboratory, UK. Data were recorded from a ~15 g sample at 1000 °C using a standard vanadium tailed furnace.

The thermal analysis of the compounds was performed on a differential thermal analysis (DTA) coupled with a thermo gravimetric analysis (TGA) apparatus (STD 2960, TA Instrument). The heating and the cooling rates of 20 °C/min were applied on approximately 80 mg of compound under air flow.

3. Results and discussion

3.1. Synthesis

The compound was prepared from La_2O_3 and WO_3 as starting oxides. Lanthanum oxide powder was dried and decarbonated at 1000 °C overnight prior to use. The oxides were weighed in

* Corresponding author. Fax: 33 2 43 83 35 06.
E-mail addresses: marie-helene.chambier.etu@univ-lemans.fr (MH. Chambrier), francois.goutenoire@univ-lemans.fr (F. Goutenoire).
[1] Current address: NIST Center for Neutron Research, National Institute of Standards and Technology, 100 Bureau Drive, Stop 6103, Gaithersburg, MD 20899, USA and University of Maryland, Dept. of Materials Science and Engineering, College Park, MD 20742, USA.

0022-4596/$ - see front matter © 2010 Elsevier Inc. All rights reserved.
doi:10.1016/j.jssc.2010.03.043

stoichiometric proportions and ground together in an agate mortar. The prepared composition was heated up to 1400 °C for one night in an alumina crucible, no particular condition was used in order to cool down the samples. This procedure was applied at least twice in order to get a stabilized compound as verified by X-ray powder diffraction. The final compound is white.

4. Crystal symmetry

From the analysis of the X-ray powder diffraction data collected on the MPD-PRO at 1000 °C, we were able to obtain good solutions from two different autoindexing programs Treor [10] and Dicvol [11] implemented in X'Pert HighScore Plus [12]. The solutions determined by the both programs are very similar: $a=12.688$ Å; $b=9.198$ Å, $c=5.985$ Å, $V=698.43$ Å^3, with a figure of merit $M_{20}=25.0$ [13] and $M_{20}=85.0$, respectively, for Treor and Dicvol.

From the average oxygen volume in oxides, $V_{oxygen}\sim 18$–22 Å^3 at room temperature, and the nominal composition $La_6W_2O_{15}$ we can estimate $Z_{max}=698.43/18/15=2.59$ and $Z_{min}=2.11$. We chose $Z=2$ leading to an oxygen volume slightly larger than the previous values, $V_{oxygen}\sim 23.3$ Å^3.

In order to determine the possible space groups of this compound, an initial procedure was performed to obtain the Bravais class. The observed intensities were extracted using a Le Bail fit in the space group *Pmmm* (No. 47). A Patterson function was then calculated with Gfou implement in the Fullprof suite. A strong peak was observed at 0.5, 0.5, 0 leading to a C orthorhombic Bravais class.

The 13 face centered orthorhombic space groups were then tested by Le Bail fitting [14] implemented in the Fullprof program [15]. These tests were done against both X-ray and neutron data for the space groups: *Cmmm* (No. 65), $C222_1$ (No. 20), *Cmma* (No. 67), *Cmmb* (No. 67), *Cmcm* (No. 63), *Ccmm* (No. 63), *Cmca* (No. 64), *Cmcb* (No. 64), *Ccma* (No. 64), *Ccmb* (No. 64), *Cccm* (No. 66), *Ccca* (No. 68), *Cccb* (No. 68). We were able to exclude ten of them: *Cmma* (No. 67), *Cmmb* (No. 67), *Cmcm* (No. 63), *Cmca* (No. 64), *Cmcb* (No. 64), *Ccma* (No. 64), *Ccmb* (No. 64), *Cccm* (No. 66), *Ccca* (No. 68) and *Cccb* (No. 68) which presented unsatisfactory profile fits. The three possible space groups *Cmmm* (No. 65), $C222_1$(No. 20) and *Ccmm* (No. 63) tested in this pattern matching mode lead to a total of nine possible centro and non-centrosymmetric space groups for the structure determination.

4.1. Crystal structure determination

As a first step, only the cation positions were sought using the X-ray diffraction data. Structure solution was determined using a Monte Carlo analysis performed by the program Espoir [16] in scratch mode, based on the first 66 low-order Bragg peaks. Intensities for these reflections peaks were extracted by a Le Bail fit in the space group *Cmmm*. Atom–atom distance constraints were used between La–W < 3.3 Å, La–La < 3.7 Å and W–W < 3.3 Å, in order to guide in the search for these atomic species. All nine possible space groups mentioned previously were tested; three of them gave *R*p around 10%, with all others yielding values for *R*p no better than 25%. For the three most promising space groups, the cation positions determined initially were then refined, leading to values of $R_{Bragg}=18.7$, 18.8 and 21.7% for the space groups $C222_1$ (No. 20), *Ccmm* (No. 63), and $Ccm2_1$ (No. 36), respectively (Table 1). Strong similarities were found between each of the cation-only solutions (Fig. 1). Subsequent attempts to determine the oxygen atom positions from the X-ray data proved difficult due to the unfavourable difference in scattering factors between W^{+6}(68 e$^-$), La^{3+}(54 e$^-$) and O^{2-}(10 e$^-$). Similar problems were also observed in this system for $La_2W_2O_9$ [17]. Nevertheless, following detailed analysis of difference Fourier maps we were able to locate 2 to 3 positions leading to 16 oxygen atoms in the structure (Table 2). Here again the three solutions were rather similar (Fig. 2). For the model in space group *Ccmm*, slight deficiencies were observed; for example, spurious oxygen positions leading to short oxygen–oxygen distances. These three incomplete models were then tested against the neutron data and, after subsequent refinements and difference Fourier analysis, the best model was obtained in space group $C222_1$ as summarized in Table 3. The whole neutron powder patterns were used in order to refine the previous structural model coming from the X-ray structural determination using the Rietveld method implemented by GSAS [18]. This model has an acceptably low weighted profile factor; however, the structural goodness-of-fit factor, R_{Bragg}, is higher than expected for such a neutron refinement although this is likely attributed to structural disorder as described below. During the refinement, many oxygen positions were obtained from the difference Fourier analysis although they invariably lead to short oxygen–oxygen distances along with an increase in the number of oxygen atoms in the unit cell. In order to address these issues, we have applied partial occupation factors to a number of

Table 1
Cation positions of α-$La_6W_2O_{15}$ obtained using Espoir and the X-ray data.

Atom	*Wyck.*	*x*	y	z
Ccmm (No. 63)				
La1	8g	0.39	0.71	0.75
La2	4c	0.09	0.5	0.75
W	4c	0.69	0.5	0.75
$Ccm2_1$ (No. 36)				
La1	8b	0.61	0.29	0.24
La2	4a	0.09	0.5	0.73
W	4a	0.69	0.5	0.76
$C222_1$ (No. 20)				
La1	8c	0.61	0.79	0.52
La2	4a	0.40	0.5	0.5
W	4a	0.19	0.5	0

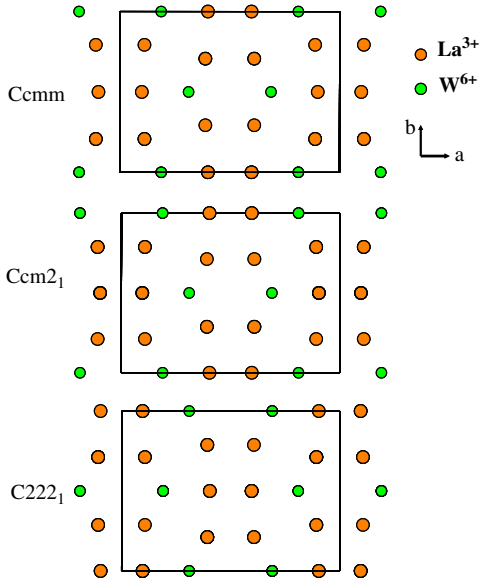

Fig. 1. Projection along *c*-axis of the three best cationic solutions. The three models are similar, it could be described by six lanthanum atoms in two by three surrounded by six tungsten atoms in a hexagonal shape.

Table 2
Partial atomic positions of α-$La_6W_2O_{15}$ obtained by Fourier-difference analysis using the X-ray data.

Atom	*Wyck.*	*x*	y	*z*
Ccmm (No. 63)				
La1	8g	0.39	0.71	0.75
La2	4c	0.09	0.5	0.75
W	4c	0.69	0.5	0.75
O1	8e	0.5	0.18	0
O2	4c	0.38	0.5	0.75
O3	4c	0.26	0.5	0.75
$Ccm2_1$ (No. 36)				
La1	8b	0.61	0.29	0.24
La2	4a	0.09	0.5	0.73
W	4a	0.69	0.5	0.76
O1	8b	0.002	0.33	0.49
O2	8b	0.32	0.29	0.26
$C222_1$ (No. 20)				
La1	8c	0.61	0.79	0.52
La2	4a	0.40	0.5	0.5
W	4a	0.19	0.5	0
O1	4b	1/2	0.31	1/4
O2	4b	0	0.14	1/4
O3	8c	0.32	0.2	0.5

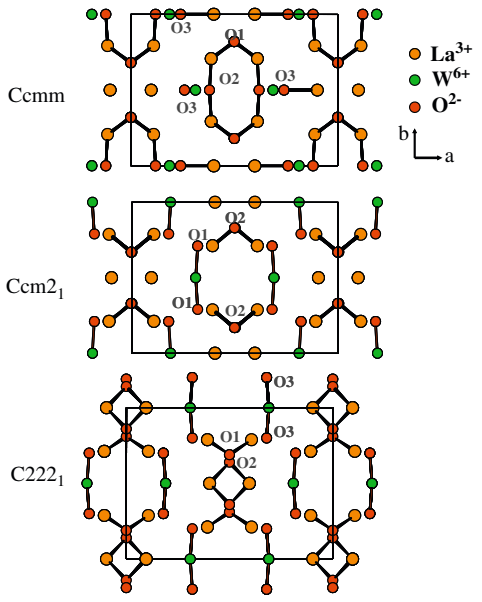

Fig. 2. Projection along *c*-axis of the three partial structure solutions deduced from powder X-ray diffraction. The oxygen in tetrahedron environment is common from the three models.

the oxygen positions, namely O3, O4, O6 and O7. The final composition has been fixed to 30. Results of the final profile fitting obtained are shown in Fig. 3. After the normalization $F(0\,0\,0)=29.2$, the final difference Fourier analysis leads to symmetric values of −0.058 and 0.057 for the residual nuclear scattering, as compare to the coherent scattering length for atomic oxygen of 0.58×10^{-12}cm.

4.2. Structure analysis

The composition $La_6W_2O_{15}$ is comparable to the formula $Bi_6Cr_2O_{15}$ and $Sb_6S_2O_{15}$ [9,19], indeed both compounds adopt the same crystal structure with the lattice parameters: $a=12.30184(5)$ Å; $b=19.87492(7)$ Å; $c=5.88162(2)$ Å for the bismuth compound. The *a* and *c* cell parameters are close to those of α-$La_6W_2O_{15}$, ($a=12.6862(3)$ Å, $c=5.9859(2)$ Å). Analysis of the $Bi_6Cr_2O_{15}$ structure and the incomplete structure of α-$La_6W_2O_{15}$ reveal similar features. The projection of $Bi_6Cr_2O_{15}$ along the *c*-axis shows $(Bi_{12}O_{14})_\infty$ columns (Fig. 4). These columns can be considered as comprising simple ribbons of tetrahedra connected by their vertices (Fig. 5a). This basic ribbon has the formula (OBi_2). The center of the ribbon is occupied by an oxygen atom with bismuth atoms above and below. $(Bi_{12}O_{14})_\infty$ columns are then made by the combination of four such ribbons. The incomplete structure obtained from the X-ray analysis of α-$La_6W_2O_{15}$ is also formed by similar simple ribbon motifs. In this

Table 3
Crystallographic parameters of α-$La_6W_2O_{15}$ obtained from Rietveld refinement against the neutron data.

Atom	*Wyck.*	*x*	*y*	*z*	$U_{iso}\times100$	s.o.f.
La1	8c	0.6094(1)	0.7891(2)	0.5117(5)	8.5(1)	1.0
La2	4a	0.0977(1)	0.0	0.0	5.6(1)	1.0
W	4a	0.1855(2)	0.5	0.0	6.2(1)	1.0
O1	4b	0.5	0.3418(4)	0.25	5.9(2)	1.0
O2	4b	0.0	0.1660(5)	0.25	9.5(3)	1.0
O3	4a	−0.1699(4)	0.0	0.0	7.1(2)	0.5
O4	8c	0.3066(4)	−0.0021(13)	0.1807(6)	8.1(2)	0.5
O5	8c	−0.1846(3)	0.2988(3)	0.5391(8)	19.7(2)	1.0
O6	8c	0.5742(5)	−0.005(2)	0.1738(8)	17.5(3)	0.5
O7	8c	0.2793(7)	0.5508(6)	0.2227(14)	16.9(3)	0.5

Bank 1 ($2\langle\theta\rangle=168°$): 108 reflections $R_{Bragg}=16.4\%$, *R*wp=8.96%; Bank 2 ($2\langle\theta\rangle=90°$): 148 reflections $R_{Bragg}=15.1\%$, *R*wp=4.26%. Space group $C222_1$ (No. 20), $a=12.6250(2)$ Å, $b=9.1875(1)$ $c=5.9688(1)$ Å, Z=2, Calculated density=6.91 g cm^{-3}; temperature=1000 °C.

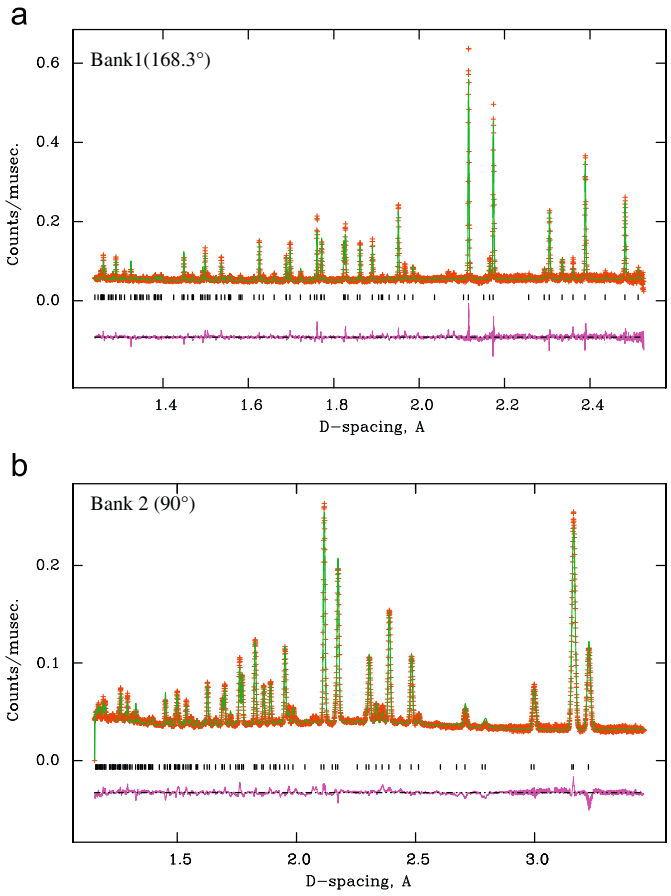

Fig. 3. Results of the final T.O.F profile refinement of $La_6W_2O_{15}$, observed cross, calculated line and difference lower profiles are shown: (a) bank 1 and (b) bank 2.

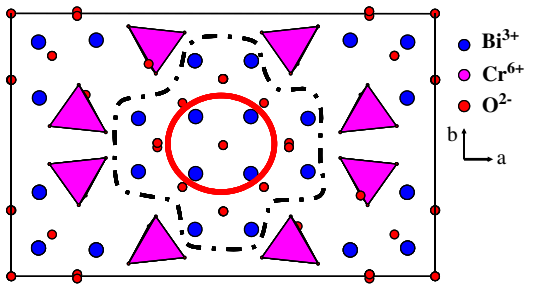

Fig. 4. Projection along *c*-axis of $Bi_6Cr_2O_{15}$, the ($Bi_{12}O_{14}$) column is surrounded by a dashed line. This column is formed by an infinite ribbon like a cross marked with a circle.

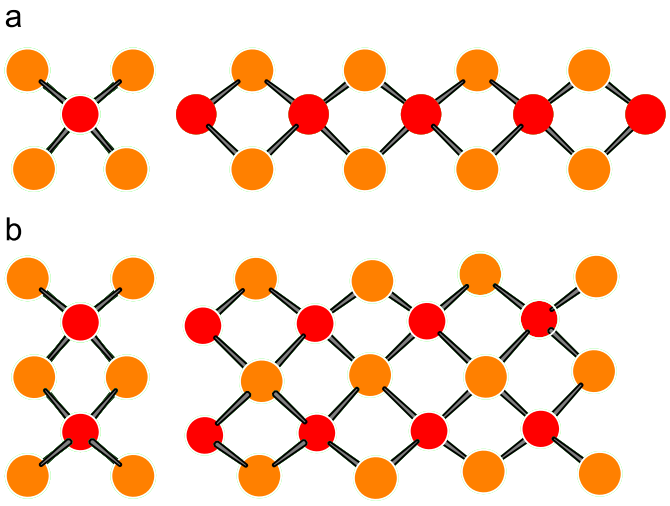

Fig. 5. Projections of a ribbon of (OA_4) tetrahedra connected by their vertices. At left faced view and at right view along the infinite direction. The global formula of such infinite ribbon is (OA_2). (b) Projections of a double ribbon. At left faced view and at right view along the infinite direction. The global formula of such infinite double ribbon is (O_2A_3).

case, two simple ribbons are combined and the formula more easily rationalized as (O_2La_3) (Fig. 5b). These types of structural features are also observed in others compounds. For example, a complex triple ribbon is observed in $Bi_{6.2}Cu_{6.2}O_8(PO_4)_3$ [20]. Perhaps surprisingly, double ribbons are even more prevalent. The ternary mixed bismuth oxides of formula BiM_2AO_6 (M=Cu, Mg, Zn, Mn, Cd, Ca, Pb; A=P, As, V) [21–24] present such double ribbons (Fig. 6a) and nearly all are described by the same orthorhombic structure in space group *Ccmm*, $a\sim12$ Å, $b\sim8$ Å and c=5.25–5.45 Å. Each of these structures made with double ribbons, triple ribbons or more complicated ribbon motifs have MO_4 tetrahedra (M=P, As or V) as their basic structural units. The compounds with double ribbons and the formula BiA_2MO_6 can be described as formed by units of formula (BiA_2O_2) or more commonly (A'_3O_2) plus isolated tetrahedra of formula (BO_4). Thus, the compound could ultimately be written as (A_3O_2)(BO_4) with the final composition as A_3BO_6 with Z=4. In order to compare such a structure with the present compound it should be formulated as $A_6B_2O_{12}$ with Z=2. A similar analysis could be made with the partial structure of α-$La_6W_2O_{15}$. The structure is formed with a double ribbon of formula $(La_3O_2)_\infty$, multiply by two leads to La_6O_4. In order to match the final composition, we have to introduce a W_2O_{11} entity. This W_2O_{11} unit must fit in only one crystallographic site, implying disorder and a possible origin of the high temperature phase transition. On ordering at low temperature, the appearance of super-structures may well be accompanied by the adoption of non-equivalent atomic tungsten

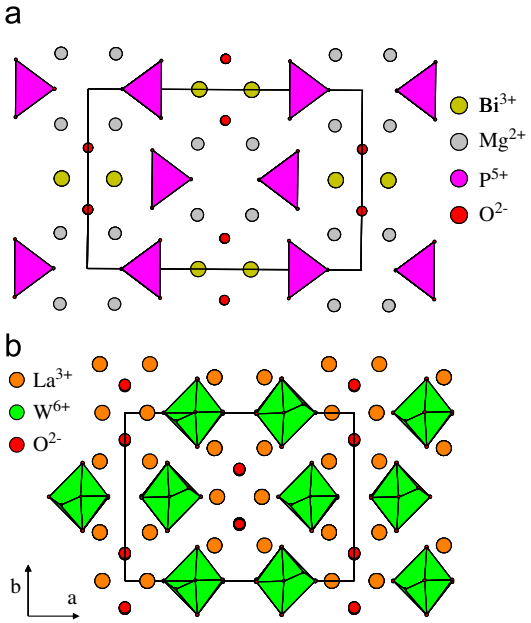

Fig. 6. (a) Projection along *c*-axis of $BiMg_2PO_6$. The chemical formula could be written as $BiMg_2O_2(PO)_4$, in order to present the (O_2BiMg_2) double ribbon and the (PO)$_4$ tetrahedra (b): M-H Chambrier projection along *c*-axis of $La_6W_2O_{15}$. The chemical formula could be written as $[La_3O_2]_2[WO_{5.5}]_2$, in order to present the (La_3O_2) double ribbon and the $WO_{5.5}$ polyhedra.

Table 4
Selected interatomic bond distances (Å) for α-$La_6W_2O_{15}$.

La1–O1	2.319(3)	La1–O5(× 2)	2.740(4)
La1–O2	2.372(3)	La1–O6(× 2)	2.801(4)
La1–O3	2.765(3)	La1–O7(× 2)	3.05(1)
La1–O4(× 2)	2.47(1)		
La2–O1(× 2)	2.421(3)	W–O3	1.826(6)
La2–O2(× 2)	2.465(3)	W–O4(× 2)	1.909(4)
La2–O4(× 2)	2.850(5)	W–O5(× 2)	1.863(3)
La2–O5(× 2)	2.965(3)	W–O6(× 2)	1.747(7)
La2–O7(× 2)	2.317(9)	W–O7(× 2)	1.840(9)

positions in the structure. A model for disorder can also be understood with the compositions $La_6W_2O_{15}$ and $A_6B_2O_{12}$, in this case $La_6W_2O_{15}$ is reformulated as $La_6W_2O_{12+3}$. Both structures BiA_2MO_6 and α-$La_6W_2O_{15}$ are represented Fig. 6a and b, respectively.

We can now understand the disorder observed during the analysis of the high temperature neutron data. The "W_2O_{11}" entity is in fact $WO_{5.5}$ because the tungsten–tungsten distance is really too large d(W–W)=5.55 Å. A true W_2O_{11} entity has been observed in this phase diagram for β-La_2WO_6 [25], formed by two corner-sharing octahedra where d(W–W)=4.13 Å.

The interatomic distances observed for this compound are summarized in Table 4. Bond valence calculations were performed manually with the atomic positions determined from the neutron refinement, using the Brown–Altermatt empirical expression: Valence=$\Sigma\exp[(Ro-d)/B]$ with B=0.37 Å [26]. The values for Ro are 2.172 Å for La^{3+}–O^2 and 1.917 Å for W^{6+}–O^2 [27]. The corresponding bond valences calculated for La1, La2 and W are 2.59, 2.99 and 6.79, respectively. These values are largely consistent with theoretical values of +3 for the lanthanum atom and +6 for the tungsten atom. The different co-ordination polyhedra around the cations should also reflect the partial occupancy of the oxygen atoms. La1 and La2 are surrounded by nine and ten oxygen atoms, respectively. As previously mentioned

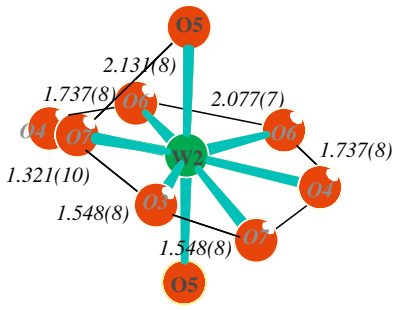

Fig. 7. Projection of the polyhedra around the tungsten atom. Atoms labelled in grey are occupied at 50%. Short oxygen–oxygen distances are marked.

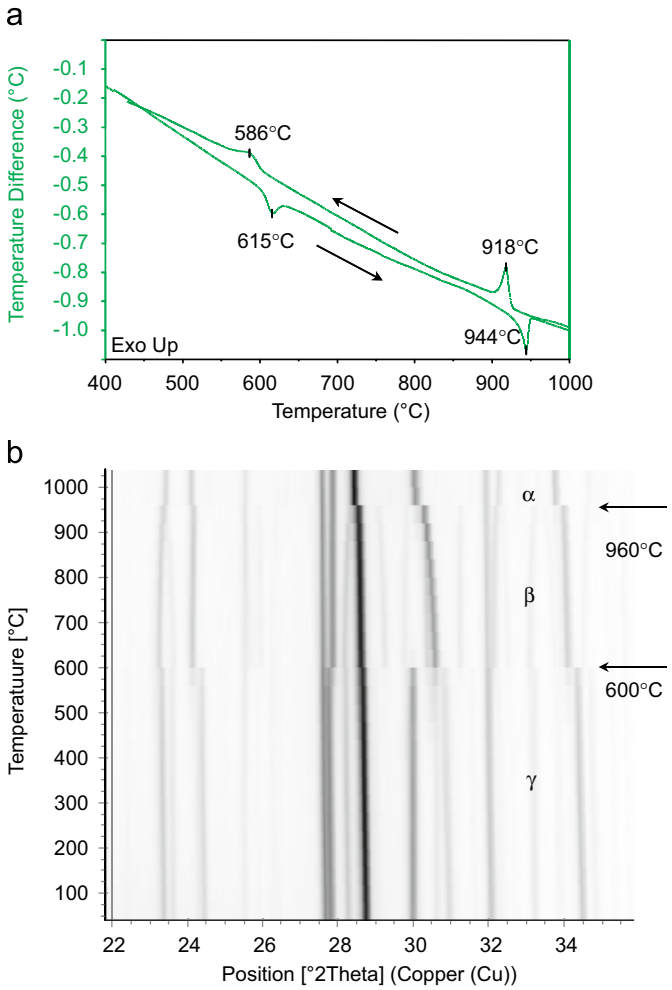

Fig. 8. (a) Differential thermal analysis of $La_6W_2O_{15}$ on heating and cooling. (b) zoom of the thermo-diffraction patterns of $La_6W_2O_{15}$ plot as a Guinier film.

in the partial X-ray structure and from the structure analysis, the tungsten atom is surrounded by 5.5 oxygen atoms (Fig. 7).

4.3. Phase transition

From the thermal analysis, two endothermic peaks were observed on heating at 615 and 944 °C that are comparable to the peaks at 630 and 930 °C observed previously (Fig. 8a). On the thermo-diffraction plot, discontinuities are also clearly observed around 600–960 °C (Fig. 8b).

The structures of the two low temperature forms are closely related to the high temperature form. Using the automatic Rietveld refinement code implemented in X'Pert HighScore Plus it was possible to refine cell parameters for both the β and γ forms using a model based on the high temperature α structure. The values obtained are given in the Supplementary information. Representative profile fit parameters are $R_{Bragg} \sim 17\%$ and 25% for the β phase and γ phase, respectively, as shown in Fig. 9. The thermal evolution of the cell volume and the cell parameters is shown in Fig. 10. Given the method of analysis, the cell parameters values should be regarded as indicative. The cell volume for $La_6W_2O_{15}$ of 670.13 Å^3 at room temperature compares with that determined by Yoshimura of 5663.32 Å^3 which leads to a ratio of 8.003.

5. Conclusion

The structure of the high temperature alpha form of $La_6W_2O_{15}$ has been determined ab-initio from in-situ thermo-diffraction X-ray powder diffraction and time-of-flight neutron powder diffraction data. The structure comprises both ordered and disordered structural motifs. The ordered part comprises an infinite ribbon of formula $(O_2La_3)_\infty$ running along the crystallographic *c*-axis. The ribbon is formed by oxygen atoms in a tetrahedral environment of lanthanum atoms of formula (OLa_4), these tetrahedra are then connected through their vertices along *c* forming an infinite ribbon of formula $(OLa_2)_\infty$. Two such adjacent ribbons are linked forming the $(O_2La_3)_\infty$ ribbons. Based on this ribbon motif we can access the nominal composition by means of: $2 \times (O_2La_3) + (W_2O_{11})$. The W_2O_{11} entity has been observed in the phase diagram for β-La_2WO_6, formed by two corner-sharing octahedra where d(W–W)=4.13 Å. In the present compound the W–W distance is too long, some 5.55 Å, leading to the second structural part of a disordered $WO_{5.5}$ unit. There are strong similarities to this disorder observed in α-$La_6W_2O_{15}$ with disorder observed in compounds of the formula BiM_2AO_6 (M=Cu, Mg, Zn, Mn, Cd, Ca, Pb; A=P, As, V).

The structure of the two low temperature forms, namely β-$La_6W_2O_{15}$ and γ-$La_6W_2O_{15}$, are closely related to the high temperature form. The structural model of the high temperature form can be used to model the main peaks of the two other crystallographic forms in the analysis on low-resolution laboratory X-ray data. From this it was possible to follow the thermal evolution of the cell parameters from room temperature to 1040 °C.

Appendix A. Supplementary data

Supplementary data associated with this article can be found in the online version at doi:10.1016/j.jssc.2010.03.043.

References

[1] M. Yoshimura, A. Rouanet, Mater. Res. Bull. 11 (2) (1976) 151–158.
[2] V.K. Yanoskii, V.I. Voronkova, Sov. Phys. Crystallogr. 20(3), 354–355.
[3] M.M. Ivanova, G.M. Balagina, E.Ya. Rode, Izv. Akad. Nauk SSSR Neorg. Mater. 6 (5) (1970) 914–919;
M.M. Ivanova, G.M. Balagina, E. Ya. Rode, Inorg. Mater. (Engl. Transl.) (1970) 803–805.
[4] F. Dubois, F. Goutenoire, Y. Laligant, E. Suard, P. Lacorre, J. Solid State Chem. 159 (2001) 228–233.
[5] V. Brizé, S. Georges, S. Kodjikian, E. Suard, F. Goutenoire, J. Solid State Chem. 177 (2004) 2617–2627.
[6] F. Goutenoire, O. Isnard, R. Retoux, P. Lacorre, Chem. Mater. 12 (9) (2000) 2575–2580.
[7] P. Lacorre, F. Goutenoire, O. Bohnke, R. Retoux, Y. Laligant, Nature 404 (2000) 856–858.
[8] D. Marrero-Lopez, J. Pena-Martınez, J.C. Ruiz-Morales, P. Nunez, J. Solid State Chem. 181 (2008) 253–262.

[9] J. Grins, S. Esmaeilzadeh, S. Hull, J. Solid State Chem. 163 (2002) 144–150.
[10] P.-E. Werner, Z. Krist. 120 (1964) 375–387.
[11] A. Boultif, D. Louër, J. Appl. Cryst. 24 (1991) 987–993.
[12] X'Pert High Score Plus, producted by PANalytical B.V., Almelo, Nerterlands, version 2.0.1, 2004.
[13] P.M. de Wolff, J. Appl. Cryst. 1 (1968) 108.
[14] A. Le Bail, H. Duroy, J.F. Fourquet, Mat. Res. Bull. 23 (1988) 447–452.
[15] J. Rodriguez-Carvajal, Program Fullprofsuite.
[16] A. Le Bail, Program Espoir 3.5, http://sdpd.univ-lemans.fr/sppd/espoir/, 2000.
[17] Y. Laligant, A. Le Bail, F. Goutenoire, J. Solid State Chem. 159 (2001) 223–227.
[18] A.C. Larson, R.B. Von Dreele, General Structure Analysis System, GSAS. Los Alamos National Laboratory, Los Alamos, NM.
[19] J.O. Bovin, Acta Crystallogr. B 32 (1976) 1771–1777.
[20] E.M. Ketatni, M. Huve, F. Abraham, O. Mentre, J. Solid State Chem. 172 (2003) 327–338.
[21] I. Radosavljevic, J.S.O. Evans, A.W. Sleight, J. Solid State Chem. 137 (1998) 143.
[22] J. Huang, Q. Gu, A.W. Sleight, J. Solid State Chem. 105 (1993) 599.
[23] F. Abraham, M. Ketatni, G. Mairesse, B. Mernari, Eur. J. Solid State Inorg. Chem. 31 (1994) 313.
[24] A. Mizrahi, J.P. Wignacourt, H. Steinfink, J. Solid State Chem. 133 (1997) 516.
[25] M.-H. Chambrier, S. Kodjikian, R.M. Ibberson, F. Goutenoire, J. Solid State Chem. 182 (2009) 209–214.
[26] I.D. Brown, D. Altermatt, Acta Cryst. B 41 (1985) 244.
[27] N.E. Brese, M. O'Keeffe, Acta Cryst. B 47 (1991) 192.